Supporting Information

Torque generation mechanism of F_1-ATPase upon NTP binding

Hidenobu C Arai*§, Ayako Yukawa*§, Ryu John Iwatate†, Mako Kamiya†, Rikiya Watanabe*‡, Yasuteru Urano† & Hiroyuki Noji*

* *Department of Applied Chemistry, School of Engineering, The University of Tokyo, Bunkyo-ku, Tokyo 113-8656, JAPAN*

† *Laboratory of Chemical Biology and Molecular Imaging, School of Medicine, The University of Tokyo, Bunkyo-ku, Tokyo 113-8656, JAPAN*

‡ *PRESTO, JST, Bunkyo-ku, Tokyo 113-8656, JAPAN*

§ *These authors contributed equally to this work.*

1, Assessment of the purity of UTP solution

Purity of UTP solution (Roche, Switzerland) was assessed using HPLC with a hydrophobic column. Nucleotides were applied on ODS-80Ts (TOSOH, Japan) equilibrated with 100 mM sodium phosphate (pH 6.9) and eluted with an isocratic flow of the buffer containing100 mM sodium phoshphate (pH 6.9) and 4 mM EDTA. We monitored the absorbance at the 260 nm wavelength (A_{260}). When we applied 100 μM UTP or 100 μM ATP, the elution profiles of A_{260} as shown in Fig. S1a were obtained. From the profiles, we identified the elusion volume of UTP and ATP as 2.3 mL and 6.0 mL, respectively. Then, to assess the contamination of ATP in UTP buffer, we independently applied three samples; 10 mM UTP without ATP (Buffer A), 10 mM UTP with 250 nM ATP (Buffer B), and 10 mM UTP with 1 μM ATP (Buffer C), and obtained the elution profiles as shown in Fig. S1b. The peak value at 6.0 mL of Buffer A is much smaller than that of Buffer B, showing that ATP contamination in Buffer A is less than 250 nM. Thus, we confirmed that 10 mM UTP buffer contained less than 250 nM ATP, which represents that ATP contamination was less than 0.0025 % of UTP. Thus, we used commercial UTP solution for a rotation assay without purification.

2, Synthesis of ribose-triphosphate (RTP)

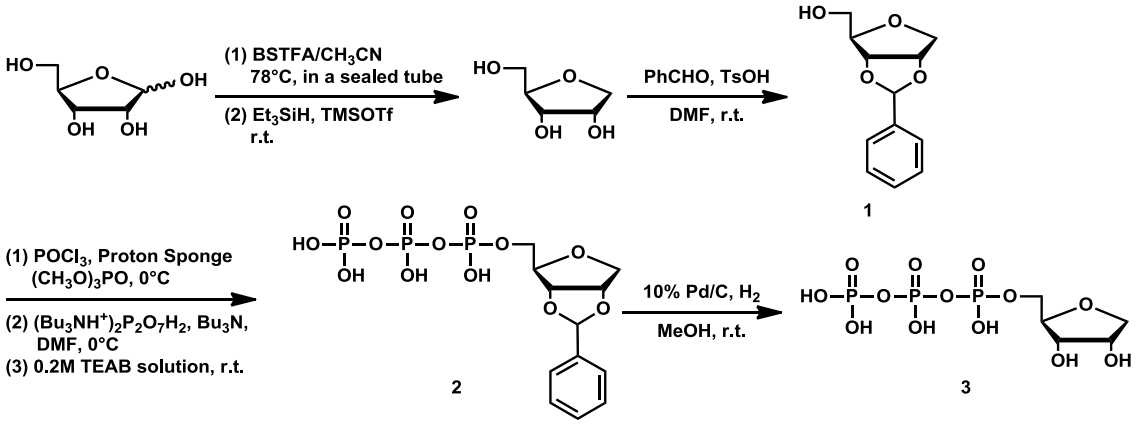

Scheme1. Synthetic scheme for ribose-triphosphate (RTP,3)

Materials and General Information. General chemicals were of the best grade available, supplied by Tokyo Chemical Industries, Wako Pure Chemical Industries, Sigma-Aldrich or Dojindo, and were used without further purification. NMR spectra were recorded on a Bruker AVANCE III 400 Nanobay at 400 MHz for ^{1}H NMR, at 101 MHz for ^{13}C NMR

and at 162 MHz for ^{31}P NMR. Chemical shifts (δ) are reported in parts per million (ppm) relative to residual solvents, TEAA or to external standard of 85% H_3PO_4. Mass spectrum (MS) was measured with a MicrOTOF (Bruker). Preparative HPLC were performed on an Inertsil ODS-3 (20.0 x 250 mm) column (GL Sciences Inc.) using an HPLC system composed of a pump (PU-2087, JASCO) and a detector (MD-2010, JASCO).

Preparation of 1,4-Anhydro-2,3-benzylidene-D-ribitol (1). 1,4-Anhydro-D-ribitol was prepared according to the literature.(1) To a solution of **1,4-Anhydro-D-ribitol** (372.1 mg, 2.48 mmol) in 7.5 ml of DMF, benzaldehyde (278 μl, 2.52 mmol, 1.02 eq) and TsOH (7.5 mg, 0.0436 mmol, 0.018 eq) were added. The reaction mixture was stirred at 70 °C for 20h, then cooled to r.t. The reaction was quenched by addition of $NaHCO_3$ (52.0 mg, 0.619 mmol, 0.25 eq), then the solvent was evaporated. The residue was dissolved in water and extracted with Et_2O. The organic layer was evaporated and purified by flash chromatography (silica gel, 5% MeOH / CH_2Cl_2) to afford 179.9 mg (0.81 mmol, yield: 32.7 %) of colorless oil. ^1H NMR (400MHz, MeOD): δ 7.53-7.51 (m, 2H), 7.38-7.36 (m, 3H), 5.77 (s, 1H), 4.86-4.84 (m, 1H), 4.72 (dd, 1H, *J* = 6.5, 1.1 Hz), 4.22-4.19 (m, 1H), 4.07-3.97 (m, 2H), 3.59-3.56 (m, 2H); ^{13}C NMR (101 MHz, MeOD): δ 137.9, 130.6, 129.2, 128.1, 107.3, 86.3, 84.3, 83.4, 73.7, 62.2; HRMS (ESI^+) Calcd for $[M]^+$, 245.07843; Found 245.07841 (-0.02 mmu).

Preparation of 2,3-Benzylidene ribose triphosphate (2). 1 (97.3 mg, 0.438 mmol) and Proton Sponge (938 mg, 4.38 mmol, 10.0 eq) were dried overnight in vacuo, and then dissolved in 12.0 ml of trimethyl phosphate. After the solution was cooled to 0 °C, 87.3 μl (0.832 mmol, 1.9 eq) of phosphorous oxychloride was added, and the reaction mixture was stirred at 0 °C for 2h. Then, a mixture of tributylammonium pyrophosphate (1326 mg, 2.80 mmol, 6.4 eq) and tributylamine (0.39 ml, 1.72 mmol, 3.9 eq) in 5 ml of DMF was added, and stirring was continued at 0 °C for additional 60 min. 5 ml of 0.2M TEAB solution was added to it, and stirred at r.t. for 1h. The reaction mixture was then lyophilized, and purified by preparative HPLC using eluent A (0.1 M TEAA buffer) and eluent B (CH_3CN 99 %, H_2O 1 %) (A/B = isocratic at 90/10 for 5 min, linear gradient to 50/50 in 40 min, isocratic at 50/50 for 10 min, then linear gradient to 90/10 in 5 min) to

afford 362.2 mg (0.0800 mmol, yield: 18.3 %) of colorless oil as TEA salt. ^{1}H NMR (400MHz, D_2O): δ 7.35-7.32 (m, 2H), 7.28-7.25 (m, 3H), 5.64 (s, 1H), 4.88-4.85 (m, 2H), 4.22-4.20 (m, 1H), 3.96-3.81 (m, 4H); ^{13}C NMR (101 MHz, D_2O): δ 131.6, 129.9, 128.1, 106.7, 84.2, 84.1, 84.0, 83.2, 74.0, 66.5; ^{31}P NMR (162 MHz, D_2O): δ -11.4 (d, 1P, *J* = 21 Hz), -11.9 (d, 1P, *J* = 19.4 Hz), -23.9 (dd, 1P, *J* = 17.2, 19.4 Hz); HRMS (ESI^-) Calcd for $[M]^-$, 460.98092; Found 460.98109 (0.17 mmu).

Preparation of Ribose triphosphate (3). 2 (18.8 mg, 0.0407 mmol) was dissolved in MeOH. 10 % palladium on carbon was added to it, and the flask was filled with H_2 using a pressurized balloon. The reaction mixture was stirred at r.t. for 2h, and then filtered through a Celite pad to remove palladium. The filtrate was concentrated and purified by HPLC to afford 10.3 mg (0.0275 mmol, yield: 67.6 %) of colorless oil. ^{1}H NMR (400MHz, D_2O): δ 4.21-4.15 (m, 2H), 4.05-3.98 (m, 3H), 3.89 (br s, 1H), 3.71-3.68 (m, 1H); ^{13}C NMR (101 MHz, D_2O): δ 81.0, 72.9, 72.1, 71.6, 66.4; ^{31}P NMR (162 MHz, D_2O): δ -11.5 (d, 1P, *J* = 17.8 Hz), -11.6 (d, 1P, *J* = 19.4 Hz), -24.0 (dd, 1P, *J* = 17.8, 19.4 Hz); HRMS (ESI^-) Calcd for $[M]^-$, 372.94962; Found 372.95151 (-1.89 mmu).

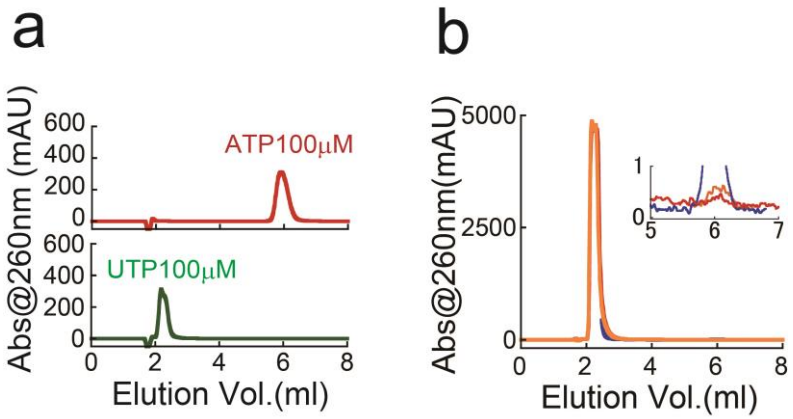

Fig. S1. Contamination of ATP in UTP solution

a. Elution profile of 100 μM ATP or UTP monitored as absorbance at 260 nm wave length.

b. Elution profile of 10 mM UTP (red), 10 mM UTP with 250 nM ATP (orange), and 10 mM UTP with 1 μM ATP (blue).

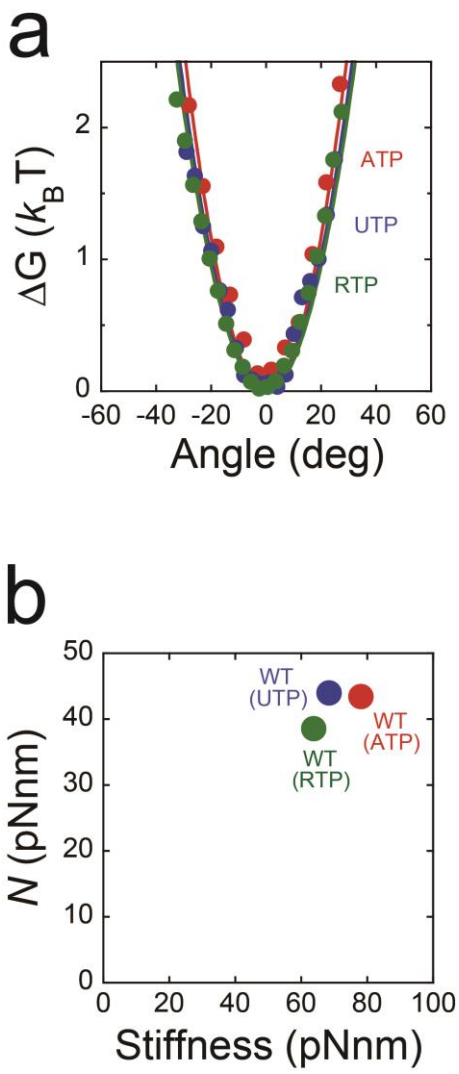

Fig. S2. Rotary potential

a. Rotary potential of the F_1 NTP waiting state. Probability distributions of angular positions during the NTP-binding pause derived from the trajectories of 3~5 molecules were transformed into rotary potentials according to Boltzman's law: wild-type F_1 with ATP (red), UTP (blue), and RTP (green). Determined potentials were fitted with the harmonic function $\Delta G = 1/2 \cdot \kappa \cdot \theta^2$, where κ is the torsional stiffness. Determined stiffness values were 79, 69, and 64 pN·nm for ATP, UTP, and RTP, respectively. **b.** Rotary torque plotted against rotary potential stiffness.

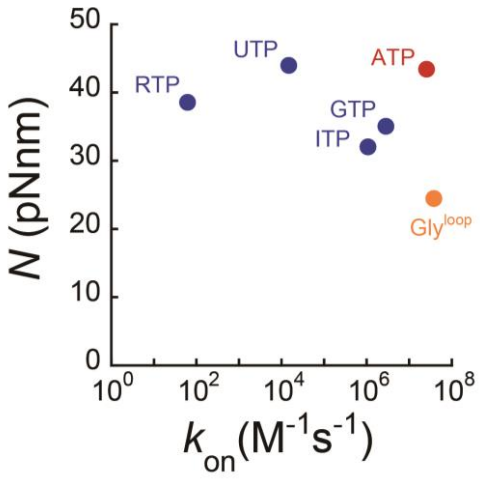

Fig. S3. Rotary torque plotted against k_{on}

Blue symbols represent the result using ATP analogs. Orange symbol represents the DELSEED mutant; $F_1^{glyloop}$ from Ref. (2).

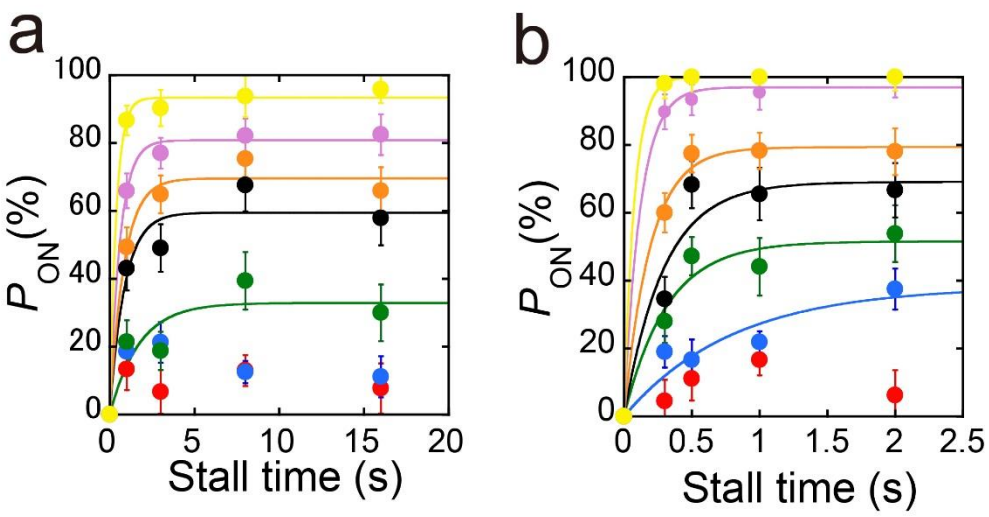

Fig. S4. Time course of P_{ON} of UTP binding at 20 and 200 μM UTP

The time course of P_{ON} of UTP binding in the presence of 20 μM (**a**) or 200 μM UTP (**b**) after stalling at –50° (red), –30° (blue), –10° (green), 0° (black), +10° (orange), +30° (pink), and +50° (yellow) from the original binding angle. These data were fitted with the same function as Fig. 4a.

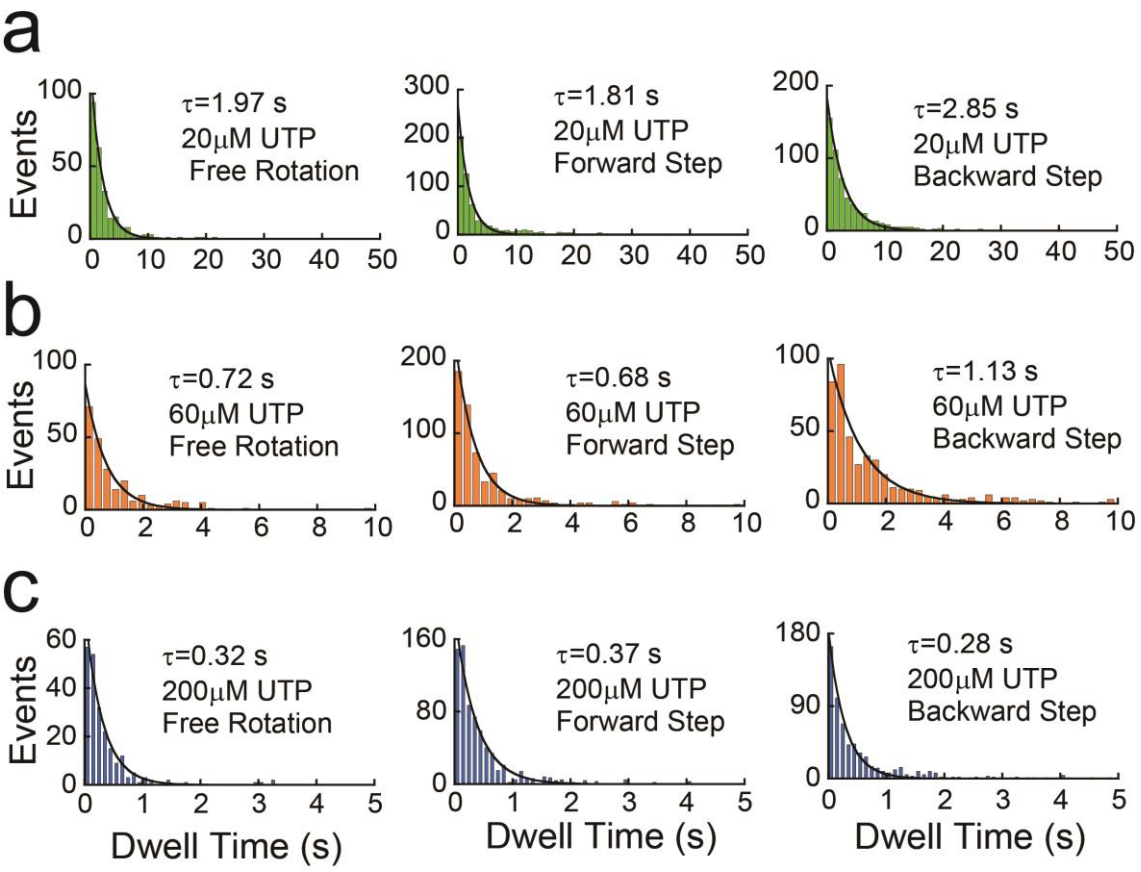

Fig. S5. Histograms of the dwell time for the UTP binding after stalling

The top row (light green: **a**), the middle one (orange: **b**) and the bottom one (blue: **c**) show the histograms at 20 μM, 60 μM and 200 μM UTP, respectively. The left column shows the histograms of binding dwells during free rotation. The middle one shows the histograms of binding dwell after the enzyme has reached the 'ON' position (Fig. 3b, left). The right one shows the histograms of binding dwells after the enzyme has reached the 'OFF' position (Fig. 3b, right). Each analysis was done for the experiments in which the stall time was long enough to reach the plateau levels in each experimental condition; 8-s and 16-s stall times for 20 μM UTP, 3-s and 5-s stall times for 60 μM UTP, and 1-s and 2-s stall times for 200 μM UTP. The time constants determined by fitting are given in each histogram.

References

1. Alfaro, J. F., T. Zhang, D. P. Wynn, E. L. Karschner, and Z. S. Zhou. 2004. Synthesis of LuxS Inhibitors Targeting Bacterial Cell−Cell Communication. Org Lett 6:3043-3046.
2. Tanigawara, M., K. V. Tabata, Y. Ito, J. Ito, R. Watanabe, H. Ueno, M. Ikeguchi, and H. Noji. 2012. Role of the DELSEED Loop in Torque Transmission of F_1-ATPase. Biophys J 103:970-978.